Petroleum Science 23 (2026) 939–953

Contents lists available at ScienceDirect

Petroleum Science

journal homepage: www.keaipublishing.com/en/journals/petroleum-science

Original Paper

Study of the effect of wax on carbon dioxide hydrate formation in oil–water mixture with high water content

Hang Yang [a,*], Jia-Qiang Jing [b,c], Jie Sun [b,c], Jia-Tong Tan [b]

[a] School of Petroleum Engineering, Chongqing University of Science and Technology, Chongqing, 401331, China
[b] School of Oil & Natural Gas Engineering, Southwest Petroleum University, Chengdu, 610500, Sichuan, China
[c] Oil and Gas Fire Protection Key Laboratory of Sichuan Province, Chengdu, 611731, Sichuan, China

ARTICLE INFO

Article history:
Received 7 April 2025
Received in revised form
25 September 2025
Accepted 28 September 2025
Available online 10 October 2025

Edited by Yan-Hua Sun

Keywords:
Hydrate nucleation
Wax
Induction period
O/W emulsion
Hydrate formation

ABSTRACT

The impact of wax on the formation of hydrates has not yet been established due to the inherent complexity of oil–water (O/W) mixtures. The O/W system has not been as extensively studied. In light of the considerations above, the present study involved the preparation of O/W emulsions through the addition of Tween-80. The investigation encompasses the impact of wax on hydrate formation in the presence or absence of Tween-80 under the influence of varying wax contents. The coupling of Tween-80 and waxes facilitated nucleation because of the heterogeneous nucleation effect of the hydrates. The induction period of hydrates first increased and then decreased with increasing wax content. At low wax content, the emulsion was in an W/O/W state, and the wax crystals precipitated in the oil encapsulated some of the water droplets, leading to a reduction of water in the outer phase of the emulsion, which was unfavorable for hydrate nucleation. Differences in the contribution of waxes to hydrate formation in non-emulsified, water-dominated and oil-dominated systems were clarified in conjunction with our previous studies. This study contributes to a comprehensive understanding of the effect of wax on hydrate formation.

1. Introduction

In multiphase mixed transport pipelines, solid-phase deposition may result in blockage, which represents a significant threat to the safe operation of these pipelines (Liu et al., 2022b; Ma et al., 2023; Melchuna et al., 2020; Xu et al., 2023). At lower ambient temperatures, waxes and hydrates may occur simultaneously (Liao et al., 2022; Liu et al., 2022c; Shi et al., 2018). They may interact with each other and affect the normal operation of the pipeline, and their interactions have received much attention from the academic community (Chen et al., 2021; Liu et al., 2022a; Song et al., 2020, 2021; Wang et al., 2020a). Studies have focused on the effect of waxes on hydrates since waxes generally precede hydrates under common experimental conditions (Liu et al., 2019; Shi et al., 2018; Tong et al., 2023; Zhang et al., 2021). Nevertheless, there is no consensus on wax's effect and mechanism on hydrates (Zhang et al., 2022). Therefore, ongoing research is necessary.

There are several key reasons why the influence of waxes on hydrate formation remains a topic of contention. It is commonly accepted that waxes facilitate the attainment of phase equilibrium in hydrates, which is thermodynamically conducive to hydrate formation (Ji, 2004; Mahabadian et al., 2016). However, the actual hydrate nucleation is more rigorous than the phase equilibrium conditions, as evidenced by an induction period for hydrate nucleation (Chen et al., 2019a; Wang et al., 2016). The original concept of the induction period was the time elapsed from phase equilibrium to the appearance of the first critical nucleus (Natarajan et al., 1994). The temperature difference between the actual nucleation and equilibrium temperatures is called subcooling (Kashchiev and Firoozabadi, 2002). This parameter is important in measuring the nucleation-driving force (Kashchieva and Firoozabadi, 2003). However, since the critical nucleation is difficult to observe, an alternative method is typically employed to determine the induction period. This method still takes phase equilibrium as the starting point of the induction period but takes the temperature increase and pressure decrease due to massive

* Corresponding author.
E-mail address: yanghang@cqust.edu.cn (H. Yang).
Peer review under the responsibility of China University of Petroleum (Beijing).

https://doi.org/10.1016/j.petsci.2025.09.042

hydrate nucleation as the end point of the induction period (Lv et al., 2015). In the analysis of the induction period, waxes exhibited both lengthening and shortening effects under different experimental conditions, which introduced uncertainty regarding the impact of waxes on hydrate nucleation (Brown et al., 2020; Jing et al., 2023b; Shi et al., 2018; Xiao et al., 2023).

The study of waxes' effects on hydrates typically involves dissolving waxes in oil, creating an oil–water two-phase system (Huang et al., 2023; Wang et al., 2024a; Zhang et al., 2021, 2023). Under agitation, this mixture can form emulsions with waxes and/or surfactants. Emulsion type depends on water content and emulsifier type (Wang et al., 2021). While crude oil contains natural emulsifiers (Raya et al., 2020), diesel and mineral oils require added surfactants to form stable emulsions for hydrate studies (Wang et al., 2024a; Zi et al., 2019). Some studies employ non-emulsified systems where oil and water are mechanically dispersed through stirring or flow (Jing et al., 2023b; Xiao et al., 2023; Zhou et al., 2018). This leads to the fact that the experimental systems are different, and although all are investigating the effect of waxes on hydrates. The systems studied include emulsifier-stabilized water-in-oil (W/O) emulsion, oil-in-water (O/W) emulsion, and stirred dispersed systems of oil–water mixture. The involvement of waxes will further complicate the system because emulsifiers may not only affect the dispersion of waxes (Ma et al., 2022) but may also adsorb at the oil–water interface to form Pickering emulsions (Gomes et al., 2024; Hajshafiei et al., 2013; Xia et al., 2021). To summarize, it is foreseeable that the effect of waxes on hydrates cannot be determined because different conclusions may be obtained in variable research systems.

Therefore, it would be irresponsible to present only the conclusion that the effect of waxes on hydrates cannot be determined, as partial agreement already exists on a more precise range. For example, the inhibitory effect of waxes on hydrates in stable wax-containing W/O systems containing emulsifiers has been widely demonstrated (Chen et al., 2019b; Liu et al., 2019; Wang et al., 2020b). For instance, experiments conducted in the cell by Wang et al. (2020b) demonstrated that wax prolongs the induction period, and the degree of inhibition is positively correlated with wax content. Their experimental system was the waxy W/O emulsion, where water droplets were stably dispersed in the oil by Span 80. Other researchers have reached the same conclusion using CH_4 and CO_2 as hydrate guest molecules in similar experimental systems (Wang et al., 2022, 2024b; Zhang et al., 2021). Chen et al., (2019b, 2021) and Jing et al. (2023c) also observed the negative effect of wax on hydrate nucleation in W/O system using cyclopentane as the hydrate guest molecule. It has been suggested that waxes adsorbed at the gas–liquid interface hinder mass transfer and negatively impact hydrate nucleation (Liu et al., 2019). There is currently a lack of studies of the O/W system. The underlying mechanism remains unelucidated and is inferred from W/O system without the benefit of tangible evidence (Wang et al., 2024a). This phenomenon suggests differences in the effect of wax on hydrate nucleation across different types of emulsions. Due to the inadequacy of the current study of waxes on hydrate formation in the O/W system, including establishing the mechanism of influence and the effect of different wax contents, a more in-depth analysis is necessary.

The dispersion of oil and water achieved by stirring without an emulsifier is poorly characterized, which leads to a lack of consensus when studying the effect of waxes on hydrate formation in this system. However, it is generally believed that small quantities of waxes favor hydrate nucleation, while high concentrations impede hydrate nucleation in the current study (Xiao et al., 2023). In contrast, some researchers maintain that waxes are always unfavorable for hydrate nucleation (Jing et al., 2023b). The mechanism remains unconfirmed, as is the case with the O/W systems. In this instance, the promotion or inhibition mechanism is inferred, but lacks evidence to support it. Since waxes need to be dissolved in oil to study the effect of waxes on hydrates. This leads to another question: the oil or water content also affect the nucleation of hydrates. It has been shown that the higher the water content, the easier it is for hydrates to nucleate when the total liquid load is kept without the addition of emulsifiers (Zheng et al., 2017). Nevertheless, this does not demonstrate that oil is detrimental to hydrate formation, as a higher water content may also influence hydrate nucleation. Thus, the impact of oil on hydrates must also be further investigated.

A predominant scenario in crude oil production is the formation of W/O emulsions, where water droplets are dispersed within a continuous oil phase. This represents the classic and most extensively studied system for hydrate risk assessment in flow assurance (Jing et al., 2023a). Water droplets dispersed in the oil phase can rapidly convert into hydrate particles, transforming a stable emulsion into a hydrate-in-oil slurry (Jing et al., 2024). Conversely, in later stages of production or in specific processing facilities, the flow regime can invert to form O/W emulsions, where oil droplets are dispersed within a continuous water phase. This scenario is particularly relevant in systems with high water cuts, which are increasingly common as oil fields mature. The continuous water phase provides an extensive network for hydrate growth, potentially leading to rapid formation of solid hydrate masses that can deposit on pipe walls or form large plugs. The mechanisms of hydrate formation, film growth, and deposition in O/W emulsions are fundamentally different from those in W/O systems and require dedicated study to develop effective mitigation strategies (Jing et al., 2025). Beyond these well-defined emulsions, real-world pipelines often handle complex and dynamic oil–water mixtures that may not form stable emulsions but rather exist as stratified or dispersed flows with evolving morphologies. Therefore, research investigating hydrate kinetics, morphology, and rheology across this spectrum—from stable W/O and O/W emulsions to transient oil–water mixtures—is of paramount practical significance.

In conclusion, further investigation is required to elucidate the impact of wax on hydrate formation. It is essential to distinguish wax's influence and the underlying mechanisms in different scenarios, thereby comprehensively delineating its effects across various systems. Due to the differential effects of wax on hydrates in W/O and O/W emulsions, the mechanism of wax influence on hydrate formation in O/W systems must be clarified. We have conducted a preliminary study examining the effect of wax on hydrates in the presence or absence of Span 80 at low water content (Jing et al., 2024). However, studies of the impact of waxes on hydrates at high water contents, particularly in O/W systems, lack both breadth and depth. Tween-80 is a nonionic surfactant with a hydrophilic-lipophilic balance (HLB) of 15. The HLB value determines emulsifier type, with values of 2–8 favoring W/O emulsions and 8–15 favoring O/W emulsions. This indicates that Tween-80 promotes O/W emulsion formation and maintains good emulsification performance under low-temperature and high-pressure conditions (Wang et al., 2024a) Therefore, this study was conducted at high water content to investigate first the impact of experimental oil on hydrate formation at constant water volume. Subsequently, the effect of wax on hydrates in the presence and absence of Tween-80 was examined, and the mechanism of action was discussed. This research will help clarify the impact of waxes on hydrates under O/W conditions.

2. Experimental section

2.1. Apparatus and materials

The hydrate formation experiments were carried out in a cell, as shown in Fig. 1. The design parameters refer to our published manuscript (Jing et al., 2024; Yang et al., 2024). The emulsion was prepared using a magnetic stirrer with a blade diameter of 5.4 cm. The microstructure of the emulsions was observed using an optical microscope of XPF-500 (Caikon Optical Instrument, Shanghai, China) with a 10x eyepiece and 10x–60x objective lens.

The preparation of emulsions requires oil, water, and emulsifiers. 3# mineral oil (Shanghai Saichu Specialty Lubricants Co., Ltd, Shanghai, China) was chosen to avoid interference from waxes, asphaltenes, resins, and other components of crude oil. The carbon number distribution of 3# mineral oil and the method for measuring the freezing point of waxy oil were described in our previous study (Jing et al., 2024). The freezing point of oils with different wax contents is shown in Fig. 2. The deionized water used for the experiment was laboratory made. The emulsion was configured using Tween-80 (AR, Jiangsu Yatai Chemical CO., Ltd), a commonly used O/W emulsifier. The #58 full-refined paraffin wax (Kunlun brand, Fushun, China) was used in the experiments. The safer and cheaper CO_2 (99.9%, Zhengrong gas, Chengdu, China) was used as a guest molecule for hydrates, as it forms hydrates with the same structure as those formed from methane.

2.2. Conditions and procedures

Hydrate formation experiments were conducted at an initial pressure of 3.10±0.01 MPa at 20 °C in all systems with a stirring rate of 500 rpm. The temperature of the experiments was controlled to 1.0 °C by a water bath. The cooling rate is 0.13 °C/min. The materials for the different hydrate experiments are shown in Table 1. The gas–liquid interface was the primary site of hydrate formation when the total liquid volume was 1.5 L and appropriate positioning of the temperature sensor. Prior to experimentation, the cell's tightness was verified using high-pressure nitrogen, and the system was thoroughly cleaned. The experimental procedure was as follows: First, the emulsion (400 mL of mineral oil and 1100 mL of water) was prepared by adding 500 ppm of Tween-80. The concentration screening of Tween-80 was shown in the appendix (Fig. S3). Mechanical stirring was performed with a rotor

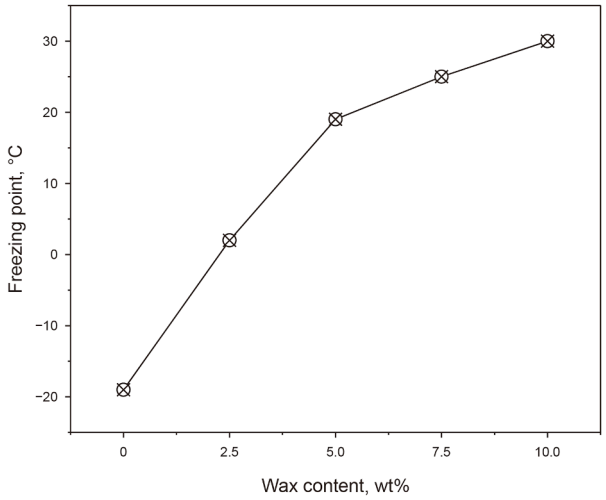

Fig. 2. Freezing point of mineral oils with different wax contents.

Table 1
The materials for the different hydrate experiments.

Experiment No.	Materials	Ratio
Exp. 1	Deionized water, CO_2	1100 mL of water
Exp. 2	Mineral oil, deionized water, CO_2	1100 mL of water, 400 mL of oil
Exp. 3	Mineral oil, deionized water, wax, CO_2	1100 mL of water, 400 mL of oil, 10 wt% wax in oil
Exp. 4	Mineral oil, deionized water, Tween-80, CO_2	1100 mL of water, 400 mL of oil, 500 ppm Tween-80
Exp. 5	Mineral oil, deionized water, wax, Tween-80, CO_2	1100 mL of water, 400 mL of oil, 500 ppm Tween-80, 10 wt% wax
Exp. 6	Mineral oil, deionized water, wax, Tween-80, CO_2	1100 mL of water, 400 mL of oil, 500 ppm Tween-80, 2.5 wt% wax
Exp. 7	Mineral oil, deionized water, wax, Tween-80, CO_2	1100 mL of water, 400 mL of oil, 500 ppm Tween-80, 5 wt% wax
Exp. 8	Mineral oil, deionized water, wax, Tween-80, CO_2	1100 mL of water, 400 mL of oil, 500 ppm Tween-80, 7.5 wt% wax

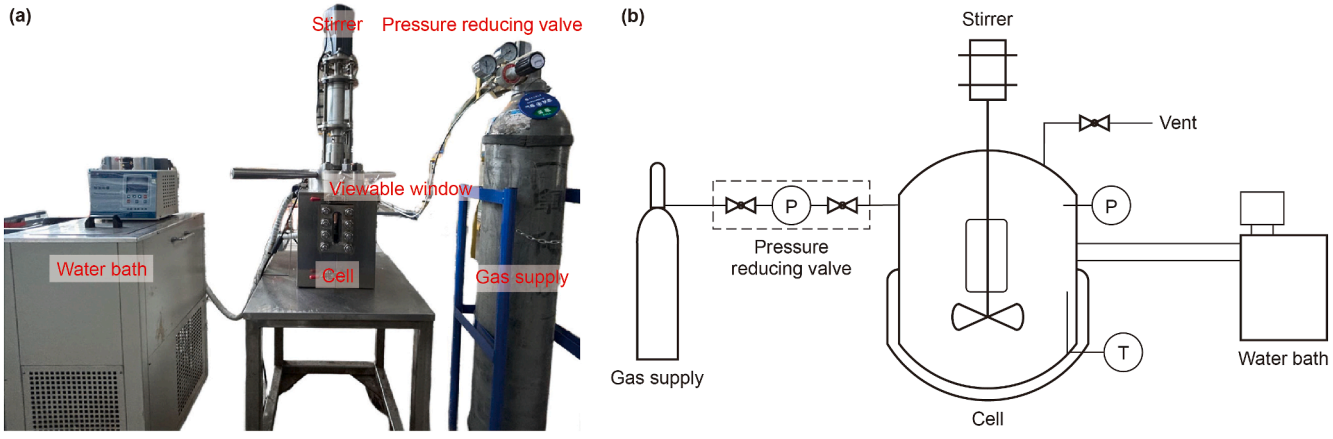

Fig. 1. Hydrate formation cell: (**a**) picture of hydrate formation apparatus, (**b**) schematic diagram of hydrate formation apparatus.

diameter of 5.4 cm, a stirring time of 30 min, and a stirring speed of 685 rpm to obtain the same linear velocity as the cell stirring. Next, the prepared emulsion was poured into the cell, and the pressure was raised to 3.10 MPa after injecting CO_2 several times to clean the air. The system was then cooled using a water bath set to 1.0 °C, with continuous cooling until hydrate formation occurred. Following complete hydrate formation, the gas was vented, and freshly prepared liquid was reinjected. This procedure was repeated three times to obtain three independent measurements of the hydrate formation induction period. The results of the repeated experiments can be found in Table S1 in the appendix. The phase equilibrium model for hydrates is Ng-Robinson, and the state equation is SRK.

3. Results and discussion

3.1. Influence of waxy mineral oil and Tween-80 on hydrate formation

3.1.1. Hydrate formation induction time and gas consumption

Previously, the effect of hydrate formation from oil was reflected in the water content. Zheng et al. (2017) maintained a constant quantity of carrier fluid and investigated the impact of mineral oil on hydrate formation under varying water content conditions. Their study found that increased water content facilitated hydrate nucleation. However, since this approach altered the water quantity, the observed enhancement in hydrate formation may simply result from the increased availability of water, rather than specifically reflecting oil's effects. To ensure experimental rigor, we maintained a constant water volume (1100 mL) across all systems, both with and without oil, as illustrated in Fig. 3. The experiments for the mineral oil–CO_2–water systems were carried out in Fig. 3(a), where the volume of oil was 400 mL and the volume of water was 1100 mL. Aluminum alloy blocks were used instead of the volume occupied by oil to exclude oil interference, as shown in Fig. 3(b). The volume of a single block was 200 mL, and two blocks were the maximum amount that could be placed. Any further increase would cause the magnetic stirrer to come into contact with the metal block thus affecting the operation of the stirrer. This constraint determined our selection of 400 mL oil volume for all experiments. Experiments for the CO_2–water system were performed in Fig. 3(c). Since the volume of oil was occupied by the metal blocks and the metal blocks were not directly involved in hydrate formation, this ensured that the amount of water and gas remained constant compared to oil-containing systems.

The induction period affected by oil, wax and Tween-80 was plotted in Fig. 4. The induction period was the shortest at 24.0 ±7.7 min in the water–CO_2 system. The addition of oil was detrimental to hydrate nucleation to 37.2±6.7 min, which was consistent with the previous conclusion (Zheng et al., 2017). The induction period was prolonged to 60.0±34.0 min by Tween-80. It suggested that Tween-80 was not favorable for hydrate nucleation. However, the system with the longest average induction period was wax–oil–water–CO_2 of 294.9±233.8 min, but the induction period shortened to 56.2±11.8 min after adding Tween-80. This phenomenon significantly differed from the Span-80, which enhances the inhibitory effect of wax (Jing et al., 2024). The findings demonstrated that using disparate emulsifiers resulted in varying effects on the nucleation of hydrates in wax-containing oil systems.

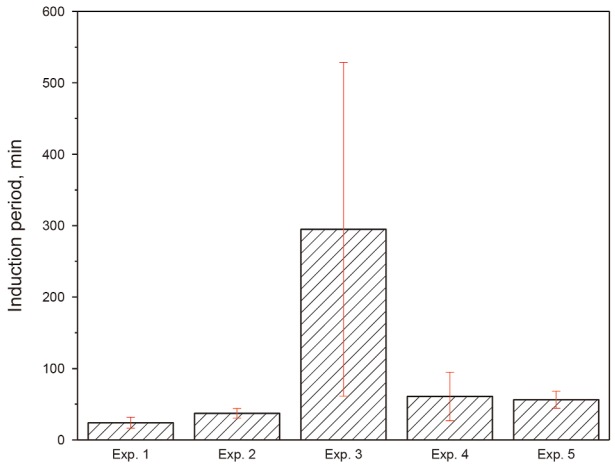

Fig. 4. Induction period influenced by mineral oil, wax, Tween-80, and their combination.

The gas consumption during hydrate formation in different systems is shown in Fig. 5. It was calculated using the same method as Liu et al. (2019). It shown that the pure water system maintained the maximum gas consumption throughout the experiment, with a final gas consumption of 0.864 mol. After adding oil, wax, and Tween-80, the gas consumption was significantly reduced, with a final gas consumption of 0.785 mol for the oil–water system, 0.688 mol for the oil–water–wax system, 0.717 mol for the oil–water–Tween-80 system, and 0.688 mol for the oil–water–wax–Tween-80 system. The final gas consumption was 0.688 mol for oil–water–wax–Tween-80 system, 0.717 mol for oil–water–Tween-80 system, and 0.688 mol for oil–water–Tween-80 system. From the view of the final gas consumption, the effects of oil, wax, and Tween-80 on the hydrate growth were basically

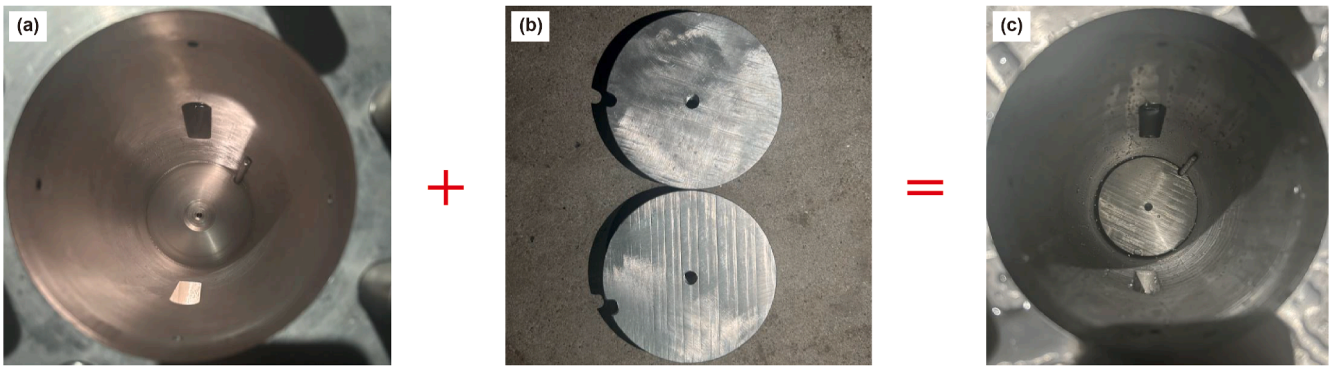

Fig. 3. The inside of the hydrate formation cell: (**a**) empty cell, (**b**) aluminum alloy block, (**c**) cell with metal blocks.

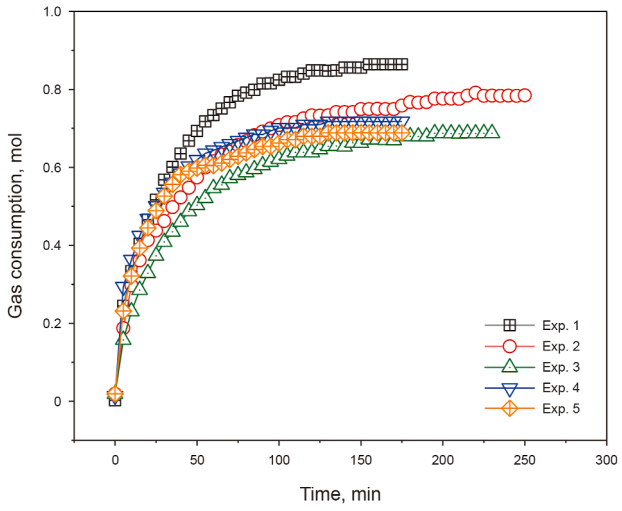

Fig. 5. Variation of gas consumption under the influence of oil, wax, and Tween-80.

the same as that of nucleation. Compared with the oil–water–wax system, the gas consumption was unchanged after the addition of Tween-80, which indicated that Tween-80 mainly promoted the hydrate nucleation but had no effect on the hydrate growth under wax-containing system. From the variation of gas consumption with time, it could be seen that for the wax-containing system, the gas consumption of hydrate was always larger than that of the wax-containing system only after the addition of Tween-80, while for the non-wax system, although the final gas consumption was smaller after the addition of Tween-80, the gas consumption was larger compared with that in the first 50 min, which was similar to that of Span-80. It indicated that Tween-80 favored the rapid growth, but would reduce the final generation.

3.1.2. Macroscopic properties of hydrate formation

Hydrate growth was observed for different systems through the visual window, as shown in Fig. 6. At the end of the induction period, hydrates began to appear. Photographs were taken to record the hydrate growth morphology of 60 min after they began to form. When the system pressure remained stable for 30 min, it was considered as the end point of growth. Fig. 6(a) showed the viewable window observation of the CO_2–water system. Hydrates were formed quickly and they grew upward along both sides of the viewable window. Then, the hydrate gradually grew from the sides towards the center, finally covering the viewable window. This phenomenon of hydrate climbing up the viewable window is similar to the observation of Liu et al. (2022c). It was because the viscosity of water was low. The stirring effect caused the liquid in the cell to swirl near the wall, which made direct contact with the gas. Moreover, the hydrate that formed at the interface tended to migrate as the hydrate formed and adsorbed to the edge of the slit at the opening of the viewable window due to the dynamic nature of the system. The homogenized liquid with Tween-80 in Fig. 6(d) and (e) had a similar formation process. Fig. 6(b) illustrates the variation in the hydrate formation of the CO_2–mineral oil–water system over the visual window. The experimental liquids exhibited inhomogeneity due to the difficulty of uniformly mixing mineral oil and water without an emulsifier. Hydrates first appeared in different morphology than homogeneous liquids. Water droplets splashed due to agitation and adhered to the viewable window. As a result of the gas, the droplets were transformed into hydrates. Hydrates can grow upward, but cannot adhere tightly to the window due to the presence of mineral oil at the interface. This similar barrier effect occurred in the equally inhomogeneous wax-containing system (Fig. 6(c)). It suggests that oil can somewhat hinder hydrate adsorption on the wall in a non-homogeneous system.

In addition to monitoring the hydrate growth process through the visual window, the cell was opened to observe the macroscopic morphology of the internal hydrate after the experiment, as illustrated in Fig. 7. Free water was still present in all systems due to the low initial system pressure setting. It was unavoidable that changes in the system's state would occur due to depressurization. These changes might potentially lead to partial hydrate decomposition. However, the results obtained could still be utilized as a reference. The venting process was relatively smooth for non-homogeneous systems, and a fast rate was used to remove all the gas as much as possible. In homogeneous systems, the presence of Tween-80 during the CO_2 discharge process resulted in the generation of a considerable quantity of foam, potentially leading to the venting pipe's freezing. Therefore, it was crucial to maintain a reasonable venting speed during this process to prevent such an occurrence. By controlling the exhaust speed of the system without Tween-80, the venting time can be maintained at approximately 20 min in all systems. It could be observed that the hydrate existed in a sheet-like aggregation state in both the gas–water and oil–gas–water systems. In contrast, hydrates were like foam under the wax–oil–gas–water system. Following the addition of Tween-80, the hydrates of wax-containing and non-wax-containing systems exhibited a more loosely packed structure. It indicated that both wax and Tween-80 were not conducive to hydrate aggregation.

3.1.3. Morphology of oil–water mixture

The macroscopic morphology of hydrates could not explain the variations in hydrate formation induction periods, as discussed in Section 3.1.1. Furthermore, direct observation of microscopic changes in gas hydrates proved challenging. Therefore, we investigated the morphology of oil–water mixtures to address this question. Fig. 8 showed the oil–water cooling and mixing simulation device. The oil–water stirring simulation experiment was conducted in a beaker, which facilitated the observation of the distribution of the liquid during the cooling process. The beaker was placed in a water bath to simulate the distribution of oil and water during the cooling process. Then, the temperature was set to the target temperature to disperse the oil and water, employing a stirrer with a direct blade of about 5.4 cm. The stirring rate was 685 rpm to obtain the same stirring linear velocity. The stirring time was 120 min to ensure that the liquid in the beaker cooled down to the target temperature. The water in the system was 275 mL, and the oil was 100 mL.

The beaker was removed from the water bath after stirring was completed, and stirring continued to be observed as fast as possible. The macroscopic morphology of the liquid was observed and photographed promptly, as illustrated in Fig. 9. It could be found that the oil and water distribution was relatively homogeneous in all the systems except for the waxy oil–water system depicted in Fig. 9(b). The white upper layer was identified as the solidified waxy oil, and the transparent layer was the water. Hydrate formation was most challenging in the waxy oil–water–CO_2 system. It was attributed to waxy oil forming a particularly thick hindering layer between the gas and water. The results of the stirring experiments could also explain the prolongation of the hydrate induction period following the addition of oil in water–CO_2 system. The presence of oil droplets at the gas–water interface during mixing resulted in the replacement of water by the oil droplets, thereby reducing the total amount of water in direct

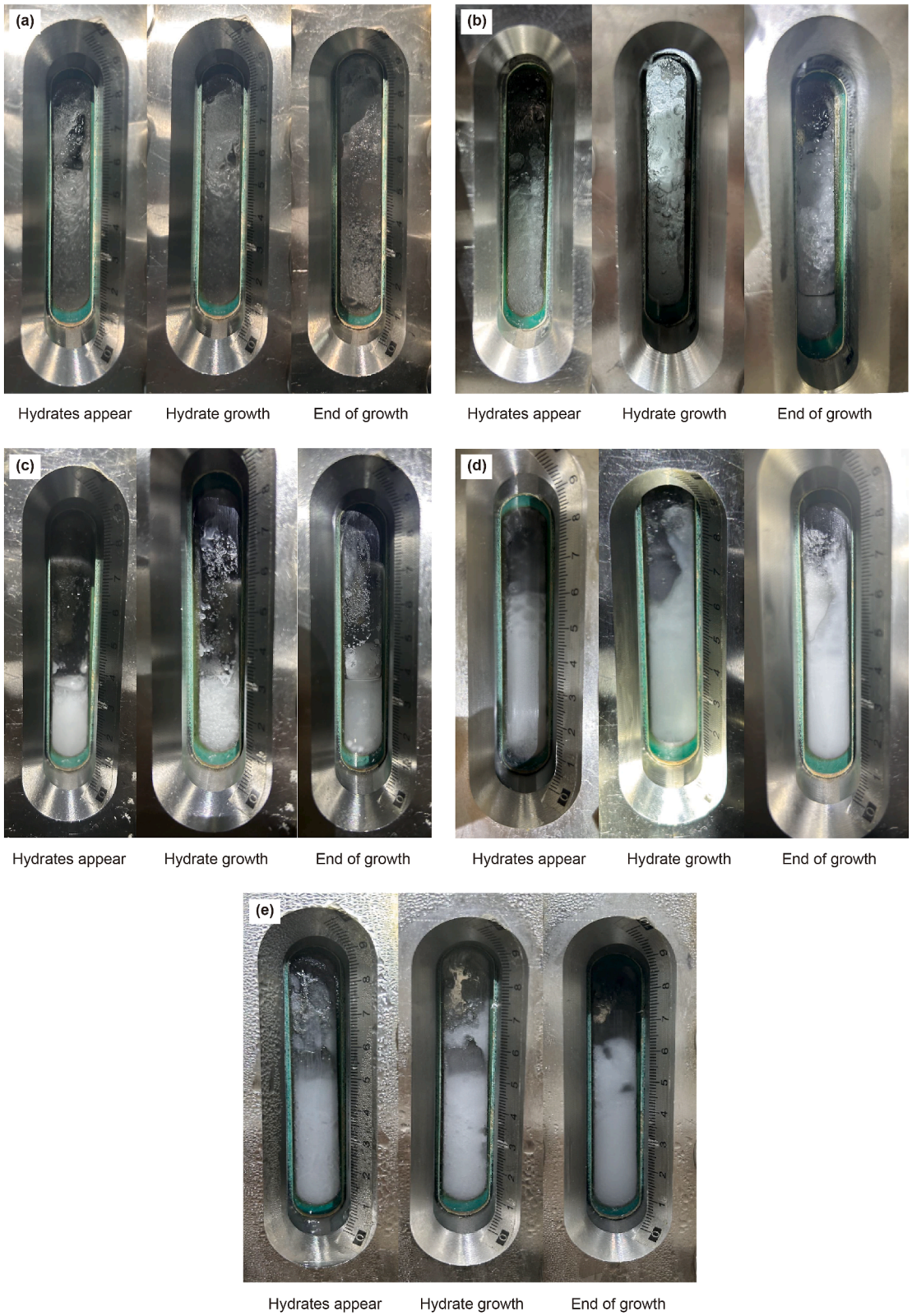

Fig. 6. Hydrate formation and growth processes in different systems: (**a**) CO_2–water system, (**b**) mineral oil–CO_2–water system, (**c**) waxy oil–CO_2–water system, (**d**) mineral oil–CO_2–water–Tween-80 system, (**e**) waxy oil–CO_2–water–Tween-80 system.

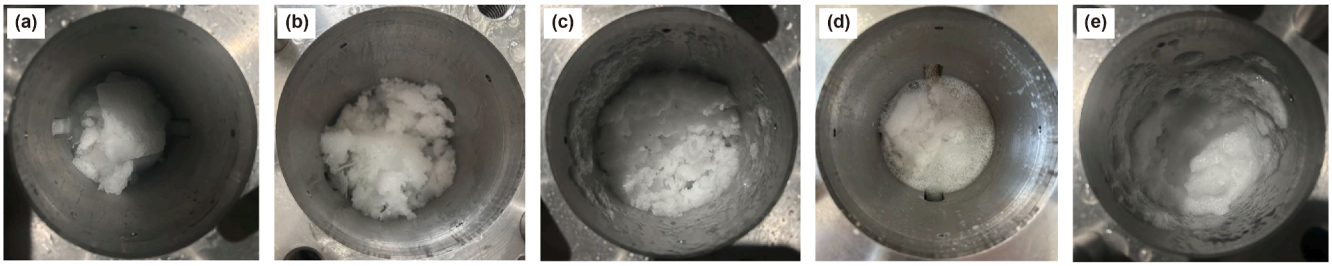

Fig. 7. Hydrate morphology inside the cell: (**a**) CO_2–water system, (**b**) mineral oil–CO_2–water system, (**c**) waxy oil–CO_2–water system, (**d**) mineral oil–CO_2–water–Tween-80 system, (**e**) waxy oil–CO_2–water–Tween-80 system.

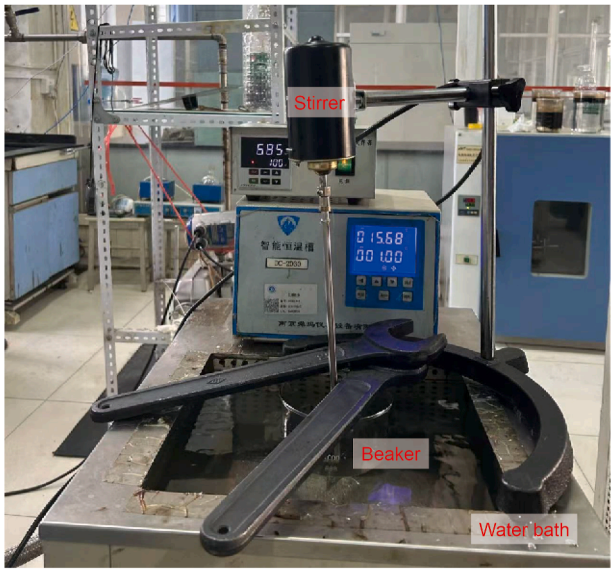

Fig. 8. Oil–water cooling and mixing device.

contact with the gas. This reduced the probability of hydrate nucleation, which in turn prolonged the induction period.

Despite the lack of explanation for the promotion of waxes in the emulsion system based on macroscopic observations, the objective was to obtain results from the microstructure of the emulsion, as illustrated in Fig. 10. The emulsion was of O/W type in the system with the addition of Tween-80 only, as shown in Fig. 10 (a). The particle size distribution of oil droplets in systems without wax and with 2.5 wt% wax was shown in Fig. S1 in the appendix. The ROImanager module of ImageJ was used to measure the particle size distribution, and a total of 336 oil droplets were identified, with an average size of 8.28 μm, a maximum size of 65.43 μm, and a minimum size of 0.76 μm, which indicates that the O/W emulsion oil droplets sampled under the combined effect of agitation and Tween-80 were more homogeneous in distribution. In comparison, the emulsion changed after the addition of 10 wt% wax. The particle size distribution of water droplets in a wax system containing 5.0–10.0 wt% was shown in Fig. S2 in the appendix. After macroscopic and microscopic observation, the mixture was divided into two parts: water with little or no encapsulated oil, and other showed a W/O morphology. Analysis of the droplet distribution using ImageJ measurements shows that the average particle size of the 229 identified droplets is 10.06 μm, with a minimum diameter of 1.08 μm and a maximum diameter of 103.42 μm. It could be categorized as a broader water-in-oil-in-water (W/O/W) emulsion. However, the oil did not take on a droplet shape. Instead, they appeared capillary. This capillary-like oil was encapsulated by water as a whole. The capillary-like appearance of the oil was because the oil was well below the freezing point and assumed a solid-like form at lower temperatures, which was stabilized in water by the action of Tween-80. This was similar to the oleogel-in-water Pickering emulsions (OPEs) (Qi et al., 2020, 2021). The low stabilizing strength of Tween-80 resulted in the oil droplets appearing to be heavily agglomerated and connected rather than dispersed as oil droplets. It was corroborated by what we found in our initial start-up experiments, where O/W emulsions were not stabilized after stopping mixing, even at addition levels above 10,000 ppm. However, the emulsion was stabilized by the synergistic effect of agitation and Tween-80. This mechanism explains the reduced hydrate induction period in wax-containing systems: Solid-like oil droplets suspended in water provided heterogeneous nucleation sites for hydrates, promoting formation compared to wax-free systems (Ji, 2004). Critically, the solid phase existed not as pure oil but as a W/

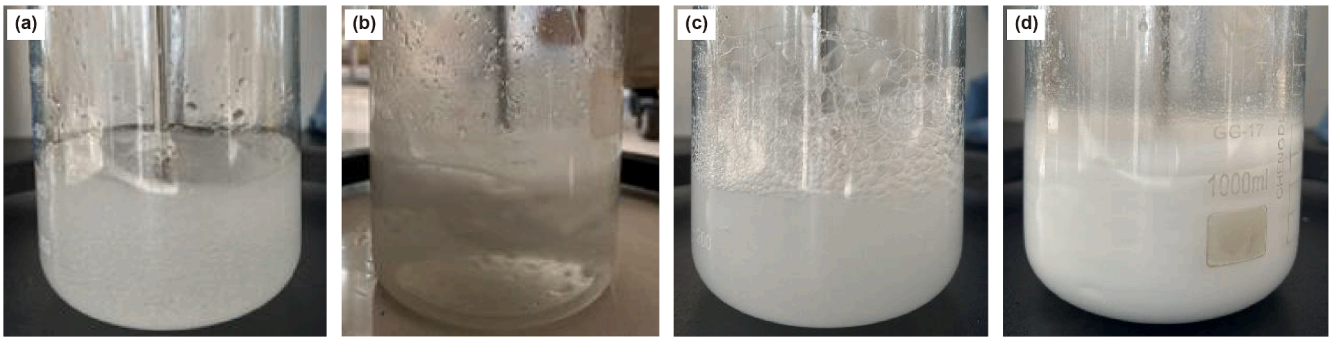

Fig. 9. Macroscopic morphology of oil and water after stirring: (**a**) mineral oil–water system, (**b**) waxy oil–water system, (**c**) mineral oil–water–Tween-80 system, (**d**) waxy oil–water–Tween-80 system.

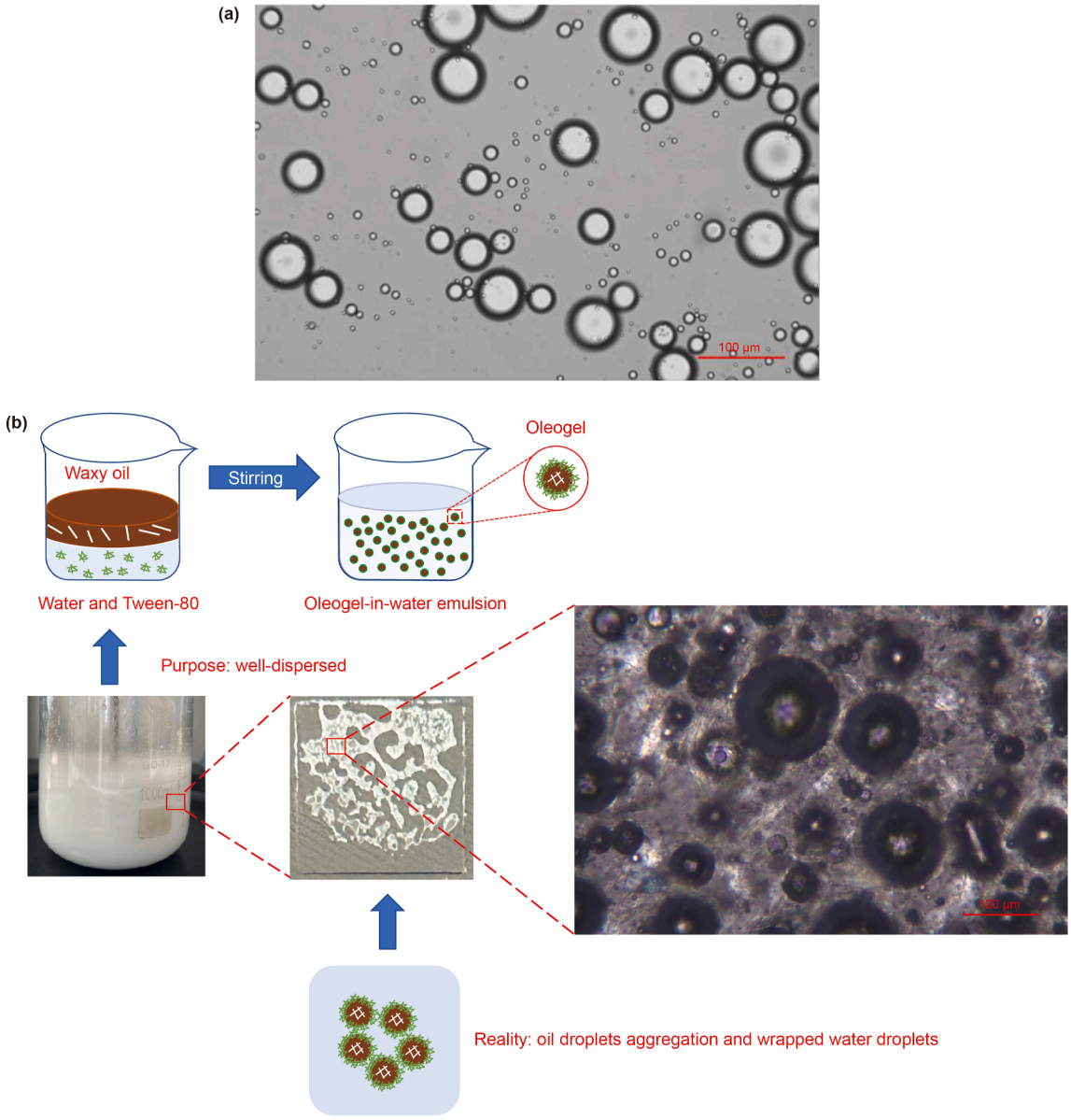

Fig. 10. Microscopic morphology of oil and water: (**a**) mineral oil–water–Tween-80 system, (**b**) waxy oil–water–Tween-80 system (green molecular: Tween-80; brown liquid: oil; light blue liquid: water).

O emulsion gel that sequestered free water. Waxes within the oil phase stabilized the oil gel structure, while waxes adsorbed at the oil–water interface stabilized the interface through Pickering emulsion formation, as shown in Fig. 10(b).

3.2. Influence of wax content on hydrate formation under O/W systems

3.2.1. Hydrate formation induction time and gas consumption

Since the effect of wax content on hydrates in emulsifier-free systems had been widely discussed (Xiao et al., 2023; Zhou et al., 2022, 2023), we only investigated the effect of wax on the induction period of hydrate formation in the presence of Tween-80. The specific experimental conditions were listed in Table 1. The average induction period under different wax content conditions was shown in Fig. 11. It indicated that lower wax content increased the average induction period, and higher levels shortened the average induction period. When the wax content was 2.5 wt%, the wax greatly prolonged the average induction period and inhibited hydrate nucleation. At a wax content of 5.0 wt%, waxes still had an inhibitory effect, although this inhibitory effect was attenuated. In contrast, at 7.5 and 10.0 wt% wax contents, the induction period shortened, demonstrating that wax promotes hydrate nucleation at higher concentrations. When considering only wax-containing systems, increasing wax content generally reduced the induction period, facilitating nucleation. However, the difference between 7.5 and 10.0 wt% wax contents was statistically insignificant, suggesting that wax's promotional effect reaches a plateau at higher concentrations.

Fig. 12 shows the temporal variation in gas consumption at different wax concentrations. When the wax content is 2.5 wt%, the trend of gas consumption of hydrate with time is basically the same compared with the wax-free system. The rate of gas consumption exhibited a notable increase prior to the 50-min mark,

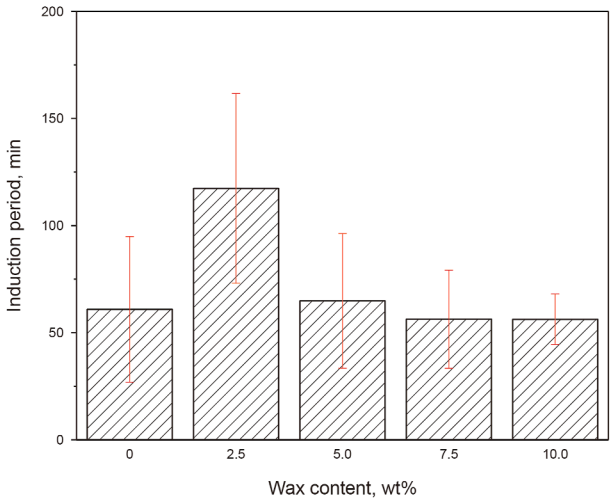

Fig. 11. Induction period of different wax contents.

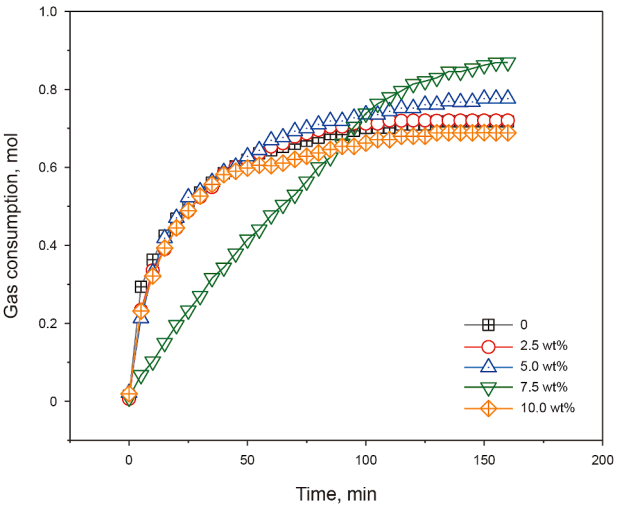

Fig. 12. Effect of wax content on gas consumption of systems containing Tween-80.

while a slight uptick was observed following the 50-min threshold. The final gas consumption was 0.717 mol for the wax-free system and 0.720 mol for the system with 2.5 wt% wax, with only a very small increase in gas consumption. The 5.0 wt% wax content was found to be generally consistent with the 2.5 wt% wax content. However, an increase in gas consumption was observed after 50 min, reaching 0.776 mol. At a wax concentration of 7.5 wt%, the observed increase in gas consumption exhibited a distinct change in trend. Initially, it was linear, rising steadily for the first 125 min. However, after this point, the rate of increase slowed down gradually. The gas consumption in this system was markedly higher than that observed in the other systems, at 0.869 mol, and exhibited an upward trend. However, it should be noted that the gas consumption was only measured for a relatively short duration of 160 min. The trend of gas consumption in the system with 10 wt % of wax was consistent with that observed in the systems with 0, 2.5, and 5 wt% wax. However, the final gas consumption was only 0.688 mol. In general, the hydrate growth tends to increase with increasing wax content and reaches a maximum at 7.5 wt%, after which the increase in wax content leads to the inhibition of hydrate growth.

3.2.2. Macroscopic properties of emulsion

Moreover, the effect of the wax on the hydrate was found to be dependent on the morphology of the emulsion. The initial step involved the observation of the emulsification of the oil–water mixture through the macroscopic approach. Fig. 13 listed the oil–water distribution of emulsions with different wax contents when stirred and left to stand for 1 min. It showed that 2.5 wt% wax content presented a clear delamination phenomenon. The emulsion exhibited a high degree of instability, as evidenced by the rapid settling of water to the bottom of the beaker. At 5 wt% wax content, the amount of water partitioning was significantly reduced, but there was still a clear oil–water interface. The oil–water interface was no longer discernible at a wax content of 7.5 wt%, and only a minimal quantity of water was separated. The emulsion was stable and homogeneous on a macroscopic scale at a 10 wt% wax content. In general, the stability of the emulsion rises as the wax content increases. This phenomenon occurred due to the precipitation of wax crystals from the oil at lower temperatures. These crystals could adsorb at the oil–water interface, thereby stabilizing the emulsion. This action had been extensively studied with the Pickering emulsion. At lower wax content, the effect of wax on the emulsion was minimal. However, with the increase in wax crystals, the effect gradually increased. The emulsion could already be stabilized for 1 min at 7.5 wt%. Observing over a longer period, we find that the emulsion can be stabilized for 30 min when the wax content is 10 wt%. This seems to correspond to the effect of wax on hydrates. The more stable this emulsion was, the better it was for hydrate nucleation.

It was also important whether the emulsion was water-continuous or oil-continuous in the presence of wax. This was first verified by adding oil and water separately in the emulsion. The addition of water did not alter the emulsion's appearance, indicating it was water-continuous. In addition, microscopic observation slides were made, as shown in Fig. 14 (10 wt% see Fig. 10). The emulsion was removed at 1 °C. The system was agitated, and the emulsion was sampled by dipping the near beaker wall through a glass rod and dropping it to the slide, subsequently covering it with a coverslip. The waxy oil was white and the water was transparent in the picture. The mineral oil was encapsulated by transparent water, proving it's an O/W emulsion consistent with the results of the dilution method. Its microstructure will be further characterized by microscopic observations in the next section, which will further determine the nature of the emulsion, thus clarifying the effect of waxes on hydrate formation.

3.2.3. Microscopic properties of emulsion

The microstructure of the emulsion was observed to further characterize the mechanism of wax on hydrate nucleation. Typical microstructures of oil–water emulsions with different wax contents were shown in Fig. 15 (10 wt% see Fig. 10). At a wax content of 2.5 wt%, the emulsion showed an W/O/W structure, as shown in Fig. 15(a). The overall presentation of the structure was predictable because Tween-80 facilitated to formation of the O/W emulsions. However, wax crystals precipitated in the oil at low temperatures. Water droplets were carried into the oil. The wax crystals trapped water droplets in the oil since they could adsorb at

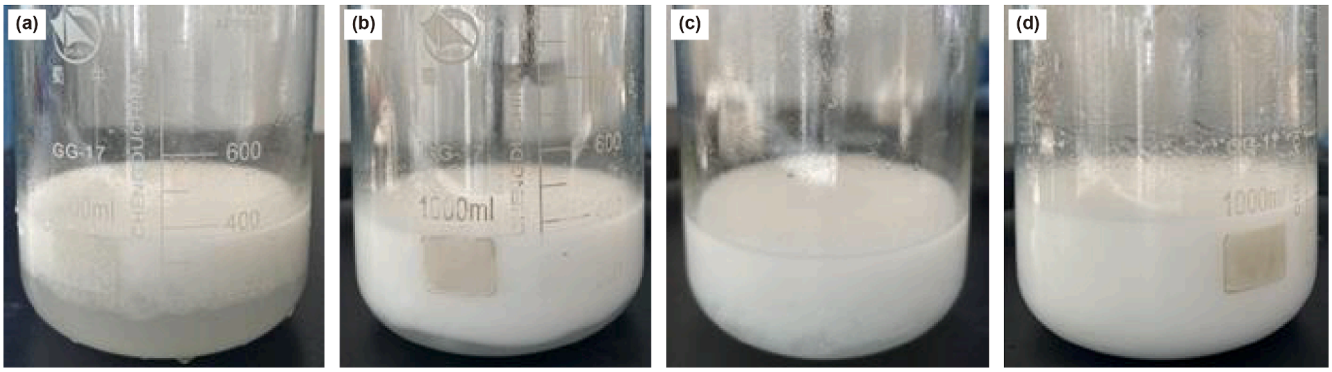

Fig. 13. Macroscopic morphology of waxy oil–water–Tween-80 under different wax content: (**a**) 2.5 wt%, (**b**) 5.0 wt%, (**c**) 7.5 wt%, (**d**) 10 wt%.

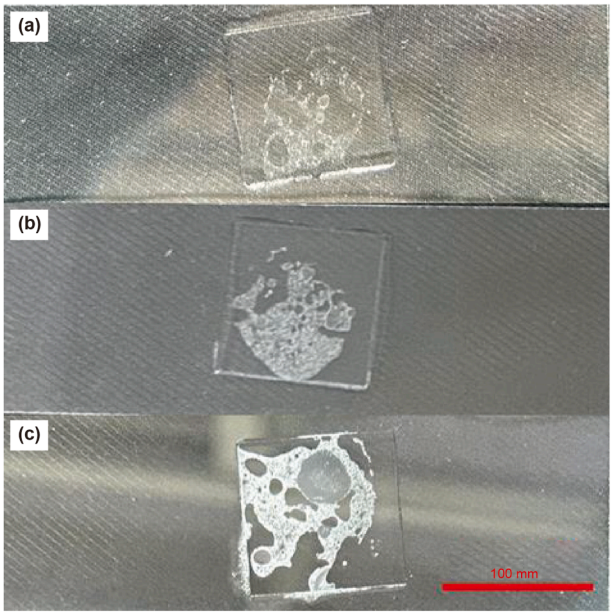

Fig. 14. Microscopic morphology of waxy oil–water–Tween-80 under different wax content: (**a**) 2.5 wt%, (**b**) 5.0 wt%, (**c**) 7.5 wt%.

the oil–water interface with agitation, thus forming an W/O/W structure. Using ImageJ to analyze the distribution of oil droplets in the system, 1157 oil droplets were identified, with an average particle size of 8.14 μm, a maximum particle size of 60.77 μm, and a minimum particle size of 0.76 μm. Compared with the wax-free system, the average particle size was reduced by 19.09 %, and the maximum particle size by 42.65 μm, which showed that the waxes were beneficial to the homogeneous dispersion of the emulsion.

When the wax content rose to 5 wt%, the oil was no longer distributed in the water as droplets. The oil was divided into two parts: one part was dispersed in the water in smaller droplets than the droplets at 2.5 wt%. The other part took on a monolithic shape. Due to the waxes' precipitation, the waxy oil's structure stabilized, solidified, and suspended in the water. The suspended oil (W/O emulsion) assumed a gelled state in the presence of a large amount of wax. In conclusion, oil–water mixtures exhibited an O/W state. The oil existed in two forms; one was the oil droplets dispersed in the water, showing a regular round (spherical) shape. The other existed as suspended gelled W/O emulsions, suspended as a whole, and encapsulated in water. Measurement of oil droplets within the continuous aqueous phase in the lower right corner using ImageJ revealed that a total of 201 oil droplets were identified, with an average particle size of 4.31 μm, a maximum particle size of 26.73 μm, and a minimum particle size of 1.479 μm, which is significantly smaller compared to the wax content of 2.5 wt% and the droplets are more dispersed in the water, and droplets at a distance are not favorable for aggregation and formation of a continuous phase.

The waxy oil encapsulated more water as the wax content continued to rise, and a continuous aqueous phase was difficult to observe throughout the field of view, as shown in Figs. 14(c) and 10 (b), which were microscopically similar for 7.5 and 10 wt% wax-containing morphology. The ImageJ was used to measure the distribution of water droplets in the continuous phase of oil. Due to the solidification of the waxy oil at low temperatures, some small droplets were difficult to distinguish, and oil droplets with diameters smaller than 3 μm and droplets that were extremely difficult to be identified were ignored in the identification process. Under the condition of 5 wt% wax content, 98 water droplets were identified, with an average particle size of 14.16 μm. Considering the water droplets as standard spheres, the total volume of oil-coated droplets was calculated to be 1.74×10^6 μm^3. The average particle size of oil-coated droplets was 18.60 μm at 7.5 wt% wax content, with a total of 134 droplets identified, and the total volume of droplets was calculated to be 3.41×10^6 μm^3. Under the condition of 10 wt% wax content, it identified a total of 142 droplets, the average particle size of 16.87 μm, with the total volume of water droplets is 3.98×10^6 μm^3. From the average particle size can be seen, the average particle size of the wax is not much different. Since the magnification is the same, the area of water droplets wrapped in oil can reflect the amount of water droplets wrapped in oil to a certain extent. The amount of encapsulated water droplets increased by 95.98% when the wax content increased from 5 to 7.5 wt%, while the amount of encapsulated water droplets increased by only a small amount as the wax content continued to increase to 10 wt%. According to the scale calculation, the image is 802 μm long and 534 μm wide, with an area of 4.28×10^6 μm^2 in the field of view, and the thickness of the observed layer in terms of the maximum particle size (139.38, 116.58, and 114.84 μm, respectively, at 5–10 wt%), in which the area of the oil phase at 5 wt% wax content is selected and calculated using the ImageJ polygon tool and the area is 2.89×10^6 μm^2, it can

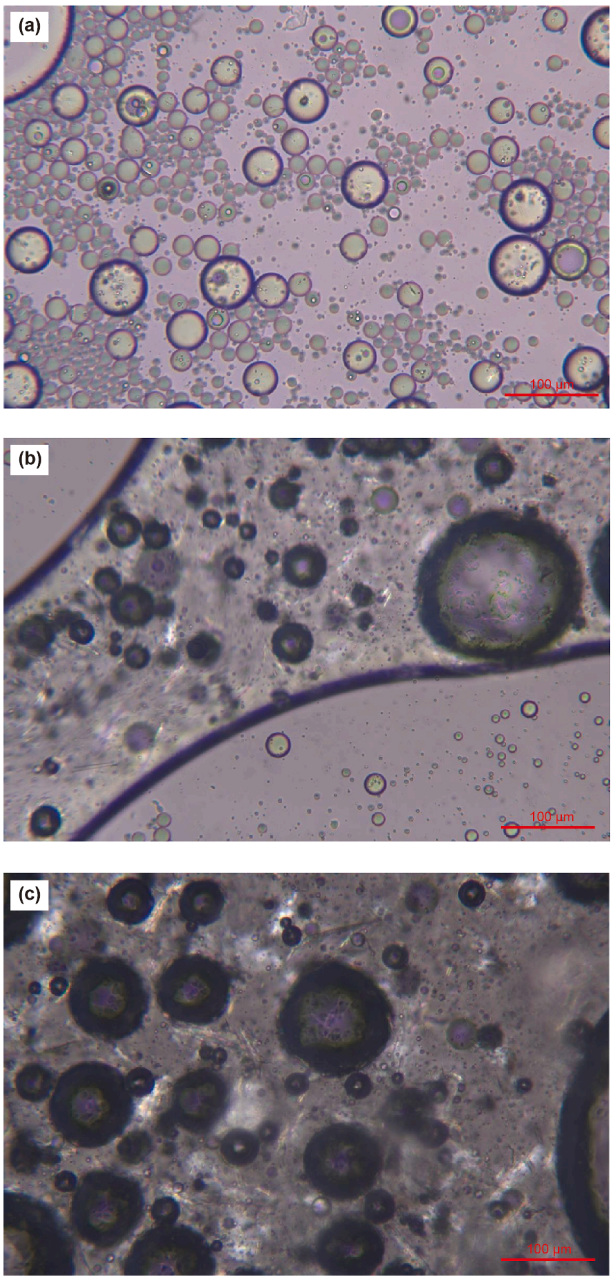

Fig. 15. Microscopic morphology of waxy oil–water–Tween-80 under different wax contents: (**a**) 2.5 wt%, (**b**) 5.0 wt%, (**c**) 7.5 wt%.

be seen that the total volume of waxy oil in the field of view is 4.03×10^7, 4.99×10^7, and 4.92×10^7 μm^3 at 5–10 wt% wax content, and the proportion of water wrapped in the oil is 4.31%, 6.83%, and 8.09%, respectively. From the total amount and percentage combined, more water droplets were encapsulated by the continuous oil phase as the wax content increased, which can explain the slowing down of the static oil–water layer with increasing wax content after stirring in Fig. 13, and the reason for this is due to the continuous water phase being absorbed and stabilized in the continuous oil phase, which resulted in the emulsion becoming better with increasing wax content on a macroscopic scale.

3.3. Hydrate formation mechanism influenced by wax

As indicated in Section 3.2, the induction period exhibited a dual trend following Tween-80 addition: it initially increased but subsequently decreased compared to the wax-free system. We conducted a study to examine the macroscopic and microscopic structures of the emulsion and to hypothesize the effect of waxes on hydrate nucleation based on their structural characteristics due to the difficulty of observing the hydrate formation process. Fig. 16 illustrated the impact of waxes on emulsions with and without Tween-80, thereby allowing for further elucidation of the mechanism by which wax influences the nucleation of hydrates. In the absence of an emulsifier, the waxy oil solidified and accumulated at the top of the liquid phase, as illustrated in Fig. 16(a). It prevented direct gas–water contact, which was detrimental to hydrate formation. Fig. 16(b) demonstrated that oil droplets could be dispersed in water in the presence of Tween-80. Wax significantly prolonged the induction period at lower wax content (2.5 wt%) in the presence of Tween-80. From the microstructure of the emulsion, the wax crystals precipitated in the oil adsorbed at the oil–water interface. The waxy oil encapsulated water droplets and changed the emulsions from O/W to W/O/W, as shown in Fig. 16(c). Further, this encapsulation effectively eliminated the free water. The nucleation probability decreased and resulted in an augmented induction period. This was similar to when adding oil. Although the total amount of water remains unchanged, hydrates were more difficult to nucleate because there is less effective water at the interface. It should be noted that at 2.5 wt% wax content, the freezing point of the waxy oil is 2 °C, whereas the average temperature at hydrate formation is 3.1 °C. It meant that wax crystals precipitated in the oil when hydrate formation, but this portion of the wax crystals could not provide hydrate nucleation sites for the successive aqueous phases because the wax crystals were encapsulated in the oil, which was in the liquid state. Moreover, from a macroscopic perspective, the emulsion could not be fully stabilized even when it contained waxes, which might result in oil–water stratification. This phenomenon occurred when the upper layer of the emulsion was dominated by oil while the lower layer was dominated by water. There was a situation where the oil isolated the gas from the water, which would be detrimental to hydrate nucleation compared to when the water was in direct contact with the gas. Thus, this combined effect resulted in the inhibition of hydrate nucleation by 2.5 wt% wax. For the 5 wt% wax content, the oil droplets no longer existed in a dispersed form. They became a continuous block, as shown in Fig. 16(d). This form differed from the standard O/W because the freezing point of waxy oil was higher than the hydrate formation temperature when the wax content was higher than 5 wt%. However, the macroscopic judgment made it possible to determine that water was the external phase. It was still an O/W emulsion. The presence of more waxes, which precipitated in the oil, made the oil appear in a gelatinous state. It was the reason for the continuous presence of the oil. As the wax crystal content rises, the water droplets become more encapsulated in the waxy oil. It was not conducive to hydrate nucleation. However, due to the heterogeneous nucleation properties of hydrates, this gelatinous continuum of oil presenting a solid state was favorable to provide sites for hydrate nucleation. This promoted hydrate nucleation. The competition between the two effects ultimately determines the effect of the wax on the hydrate. At a wax content of 5 wt%, wax's inhibition of hydrate nucleation is due to a stronger impact of reduced water volume. As

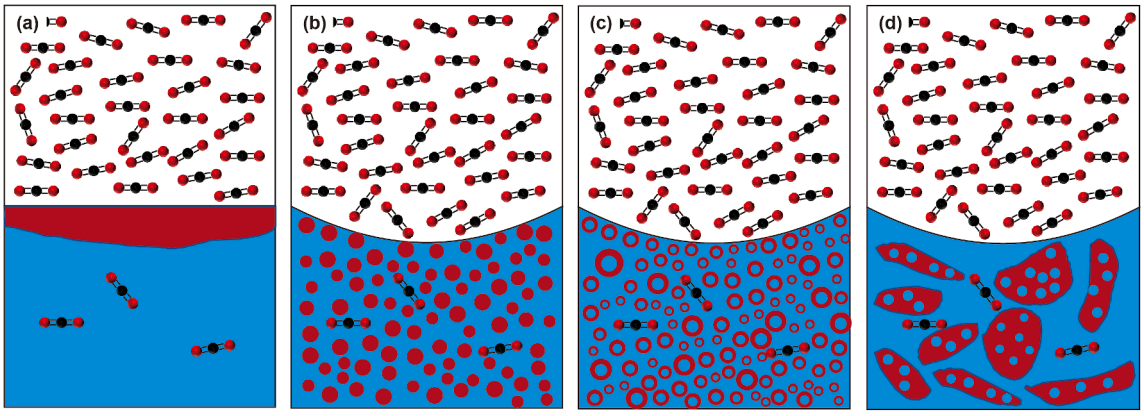

Fig. 16. Distribution of emulsions of different systems in the cell: (**a**) wax only, (**b**) Tween-80 only, (**c**) lower wax content, (**d**) higher wax content. The red circles in the diagram are oxygen atoms, the black circles are carbon atoms, the dark red color is oil, and the light blue is water.

the wax crystal content increased, the hydrate heterogeneous nucleation effect gradually dominated and eventually promoted hydrate nucleation. This explains the effect of wax on hydrate nucleation in the range of 5–10 wt% wax content. In contrast, at 2.5 wt% wax content, heterogeneous nucleation was negligible, resulting in a significantly longer induction period than other conditions.

3.4. Comparison of wax distribution and effect on hydrate formation in varying oil–water systems

Oil–water mixtures could be classified into three distinct categories: non-emulsified systems, W/O emulsion systems, and O/W emulsion systems. In conjunction with a previous study (Jing et al., 2024), a summary of the five possible forms of wax was provided herein. This finding indicated that the various forms of wax present in oil–water mixtures exert distinct effects on hydrate formation, as illustrated in Fig. 17. When water droplets were dispersed in the oil phase, wax crystals adsorbed at the oil–water interface (WAX-I) or aggregated in the oil phase (WAX-II). This phenomenon hindered the diffusion of gas from the oil phase into water droplets, leading to a mass transfer inhibition effect. As the oil droplets were dispersed in the aqueous phase, a large number of wax crystals precipitated (WAX-III) at low temperatures leading to gelling of the waxy oil. The solid phase wax/gelatinized oil droplets facilitated heterogeneous nucleation of hydrates.

In oil-dominated systems, as depicted in Fig. 17(b), the incorporation of an emulsifier led to a modification in the distribution pattern of the wax crystals. This alteration resulted in the complete encapsulation of water droplets at high wax concentrations, a condition that was not conducive to the processes of hydrate nucleation and aggregation. The distribution of waxes in the water-dominated system is illustrated in Fig. 17(c). The presence of wax crystals or agglomerates was evident at the water–oil interface of wax-containing O/W emulsions, as illustrated in WAX-V. The distribution of wax crystals within the oil phase was observed, and at low wax contents, the crystals were found to stabilize water droplets at low temperatures, leading to the formation of an W/O/W emulsion. Additionally, some of the outer-phase water was encapsulated by the oil droplets, which resulted in a reduction of the continuous aqueous phase. This led to a decrease in the nucleation probability of the hydrate and showed inhibition to hydrate nucleation. When the wax content was high, the wax crystals form a lattice structure in the aggregated oil droplets. This structure was relatively stable, and the stirring action could not destroy them into water droplets. As a result, they were suspended in water as a solid whole at low temperature. This is favorable to the heterogeneous hydrate nucleation.

The underlying cause of the inability to ascertain the effect of waxes on hydrates is the presence of waxes in diverse forms within oil–water mixtures. The most fundamental reason for this complexity is the inherent complexity of the liquid phase. The presence of emulsifiers further complicates the matter, resulting in wax morphology that is more difficult to predict. Consequently, elucidating the impact of waxes on hydrate formation necessitates a comprehensive examination of the oil–water distribution within the system.

4. Conclusions

This study investigates the effects of waxes on hydrate nucleation under the combined influence of Tween-80 and wax, complementing existing research on wax-related hydrate nucleation. It enables a comprehensive examination of wax impacts across different systems: W/O emulsions, O/W emulsions, and additive-free dispersed liquids under stirring. By clarifying wax effects under varied conditions, this work challenges the widely accepted but indeterminate conclusion that wax effects on hydrate nucleation are non-deterministic. We obtained the following findings.

(1) Oil is unfavorable for hydrate nucleation at a certain total water content. The reason for this is that hydrates nucleate at the gas–liquid interface. Oil will inevitably be present at the oil–water interface due to the addition of oil, which reduces the quantity of water in direct contact with the gas and diminishes the probability of nucleation, thereby extending the induction period.
(2) Both waxes and Tween-80 were detrimental to hydrate nucleation, but the coexistence of waxes and Tween-80 had a shorter induction period than when they were present

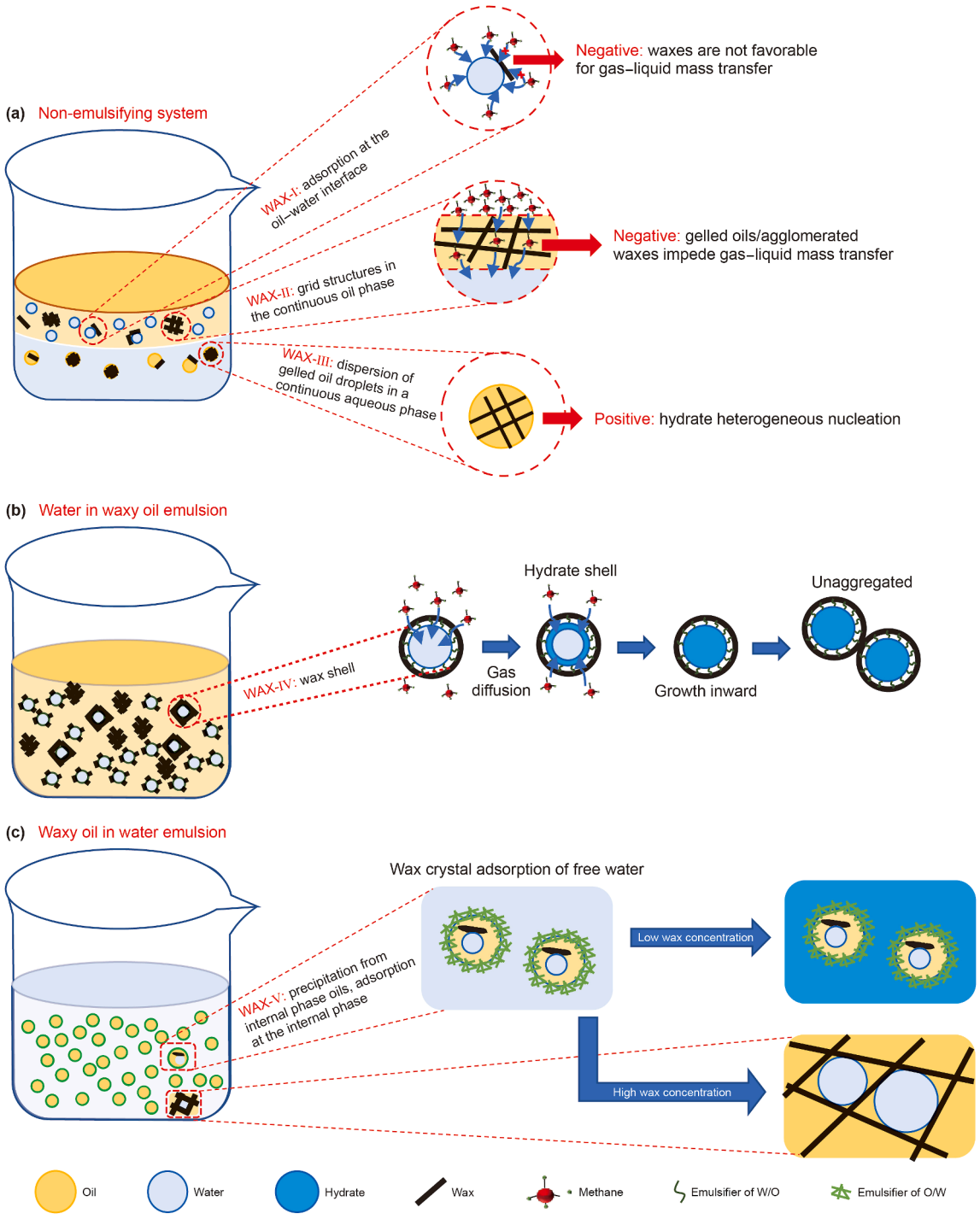

Fig. 17. Wax distribution and effect on hydrate formation: (**a**) non-emulsifying systems, (**b**) W/O, (**c**) O/W.

alone, and the order of the induction period was wax only > Tween-80 only > coexistence. The longest induction period for wax-only systems is because waxy oils solidify at low temperatures and are suspended above the water due to their lower density, separating the oil from the water. The shortening of the induction period when wax and Tween-80 coexist is because freezing waxy oil favors heterogeneous nucleation of the hydrate.

(3) With the addition of Tween-80, the induction period tended to increase and then decrease compared to the blank group. If the blank group is not considered, the induction period of hydrate is shortened with the increase in wax content. Since waxes facilitate the formation of Pickering emulsions, when the wax content is low, it does not allow the oil to solidify completely. The oil is dispersed in the water as oil droplets, and the waxes precipitated in the oil facilitate the stabilization of the water, resulting in the formation of W/O/W emulsions. As there is less water in the outer phase, the chances of nucleation are reduced, which is detrimental to hydrate nucleation. However, as the wax content rises, the waxy oil exists as a continuous solid phase, which facilitates heterogeneous nucleation of the hydrate, and a sufficiently

high wax content counteracts the inhibition brought about by the encapsulated water, thus exhibiting nucleation facilitation. This confirms a difference between wax's effect on hydrate nucleation in the O/W and W/O systems.

CRediT authorship contribution statement

Hang Yang: Writing – review & editing, Writing – original draft, Methodology, Investigation, Conceptualization. **Jia-Qiang Jing:** Writing – review & editing, Funding acquisition, Data curation, Conceptualization. **Jie Sun:** Visualization, Validation, Investigation. **Jia-Tong Tan:** Validation, Data curation.

Declaration of competing interest

The authors declare that they have no known competing financial interests or personal relationships that could have appeared to influence the work reported in this paper.

Acknowledgments

This project is financially supported by the National Natural Science Foundation of China (Grant Nos. 52106208, U19B2012), the Natural Science Foundation of Sichuan Province (Grant No. 24NSFSC6775, 2023NSFSC0924) and Central Government Guided Local Science and Technology Development Fund Project (Grant No. 2024ZYD0123).

Appendix A. Supplementary data

Supplementary data to this article can be found online at https://doi.org/10.1016/j.petsci.2025.09.042.

References

Brown, E.P., Turner, D., Grasso, G., et al., 2020. Effect of wax/anti-agglomerant interactions on hydrate depositing systems. Fuel 264, 116573. https://doi.org/10.1016/j.fuel.2019.116573.

Chen, J., Chen, G.J., Yuan, Q., et al., 2019a. Insights into induction time and agglomeration of methane hydrate formation in diesel oil dominated dispersed systems. Energy 170, 604–610. https://doi.org/10.1016/j.energy.2018.12.138.

Chen, Y.C., Shi, B.H., Liu, Y., et al., 2019b. In situ viscosity measurements of a cyclopentane hydrate slurry in waxy water-in-oil emulsions. Energy & Fuels 33 (4), 2915–2925. https://doi.org/10.1021/acs.energyfuels.8b04268.

Chen, Y.C., Shi, B.H., Fu, S.K., et al., 2021. Kinetic and rheological investigation of cyclopentane hydrate formation in waxy water-in-oil emulsions. Fuel 287, 119568. https://doi.org/10.1016/j.fuel.2020.119568.

Gomes, V.R., Martinez-Villabona, O.J., de Paiva, L.C., et al., 2024. Pickering stabilization of water-in-crude oil emulsions by paraffin wax crystals: Insights from X-ray scattering. Colloids Surf. A Physicochem. Eng. Asp. 688, 133619. https://doi.org/10.1016/j.colsurfa.2024.133619.

Haj-shafiei, S., Ghosh, S., Rousseau, D., 2013. Kinetic stability and rheology of wax-stabilized water-in-oil emulsions at different water cuts. J. Colloid Interface Sci. 410, 11–20. https://doi.org/10.1016/j.jcis.2013.06.047.

Huang, B., Li, J.Y., Fu, C., et al., 2023. Rheology investigation of propane gas hydrate crystallization in water/asphaltene-resin-wax deposit emulsions. J. Dispersion Sci. Technol. 44 (9), 1637–1646. https://doi.org/10.1080/01932691.2022.2032134.

Ji, H.Y., 2004. Thermodynamic Modelling of Wax and Integrated wax-hydrate. Doctoral Dissertation. Heriot-Watt University.

Jing, J.Q., Guo, Y.Y., Karimov, R., et al., 2023a. Drag reduction related to boundary layer control in transportation of heavy crude oil by pipeline: A review. Ind. Eng. Chem. Res. 62 (37), 14818–14834. https://doi.org/10.1021/acs.iecr.3c02212.

Jing, J.Q., Zhuang, L.Q., Karimov, R., et al., 2023b. Investigation of natural gas hydrate formation and slurry viscosity in non-emulsifying oil systems. Chem. Eng. Res. Des. 190, 687–703. https://doi.org/10.1016/j.cherd.2023.01.017.

Jing, J.Q., Zhuang, L.Q., Karimov, R., et al., 2023c. Rheology properties of cyclopentane hydrate slurry in the presence of wax crystals. Energy Sources, Part A Recovery, Util. Environ. Eff. 45 (3), 7629–7647. https://doi.org/10.1080/15567036.2023.2224740.

Jing, J.Q., Yang, H., Sun, J., et al., 2024. Study on the effect of wax on hydrate formation in the presence/absence of Span 80. J. Mol. Liq. 403, 124853. https://doi.org/10.1016/j.molliq.2024.124853.

Jing, J.Q., Yang, H., Sun, J., et al., 2025. Potential kinetic effects of wax on clathrate hydrate formation: A review. Geoenergy Sci. Eng. 249, 213765. https://doi.org/10.1016/j.geoen.2025.213765.

Kashchiev, D., Firoozabadi, A., 2002. Driving force for crystallization of gas hydrates. J. Cryst. Growth 241 (1–2), 220–230. https://doi.org/10.1016/S0022-0248(02)01134-X.

Kashchieva, D., Firoozabadi, A., 2003. Induction time in crystallisation of gas hydrates. J. Cryst. Growth 250 (3–4), 199–515. https://doi.org/10.1016/S0022-0248(02)02461-2.

Liao, Q.Y., Shi, B.H., Song, S.F., et al., 2022. Molecular insights into methane hydrate growth in the presence of wax molecules. Fuel 324, 124743. https://doi.org/10.1016/j.fuel.2022.124743.

Liu, J., Wang, J., Dong, T., et al., 2022a. Effects of wax on CH_4 hydrate formation and agglomeration in oil-water emulsions. Fuel 322, 124128. https://doi.org/10.1016/j.fuel.2022.124128.

Liu, Y., Shi, B.H., Ding, L., et al., 2019. Study of hydrate formation in water-in-waxy oil emulsions considering heat transfer and mass transfer. Fuel 244, 282–295. https://doi.org/10.1016/j.fuel.2019.02.014.

Liu, Y., Lv, X.F., Ma, Q.L., et al., 2022b. Investigation on synergistic deposition of wax and hydrates in waxy water-in-oil (W/O) flow systems. Pet. Sci. 19 (4), 1840–1852. https://doi.org/10.1016/j.petsci.2022.04.004.

Liu, Z.M., Geng, X., Gao, Y., et al., 2022c. Effect of wax crystal on the kinetic and morphology of gas hydrate deposition in water-in-oil emulsions. Fuel 330, 125501. https://doi.org/10.1016/j.fuel.2022.125501.

Lv, X.F., Shi, B.H., Wang, Y., et al., 2015. Experimental study on hydrate induction time of gas-saturated water-in-oil emulsion using a high-pressure flow loop. Oil Gas Sci. Technol. Revue d'IFP Energies Nouvelles 70 (6), 1111–1124. https://doi.org/10.2516/ogst/2014032.

Ma, Q.L., Liu, Y., Lv, X.F., et al., 2022. In situ record of the dynamic process of wax deposition in water-in-oil emulsion: Evolution of two types of deposition structures. J. Petrol. Sci. Eng. 214, 110560. https://doi.org/10.1016/j.petrol.2022.110560.

Ma, Q.L., Wang, C.S., Lu, Y.D., et al., 2023. Water droplets tailored as wax crystal carriers to mitigate wax deposition of emulsion. ACS Omega 8 (8), 7546–7554. https://doi.org/10.1021/acsomega.2c06809.

Mahabadian, M.A., Chapoy, A., Burgass, R., et al., 2016. Mutual effects of paraffin waxes and clathrate hydrates: A multiphase integrated thermodynamic model and experimental measurements. Fluid Phase Equilib. 427, 438–459. https://doi.org/10.1016/j.fluid.2016.08.006.

Melchuna, A., Zhang, X., Sa, J.-H., et al., 2020. Flow risk index: A new metric for solid precipitation assessment in flow assurance management applied to gas hydrate transportability. Energy & Fuels 34 (8), 9371–9378. https://doi.org/10.1021/acs.energyfuels.0c01203.

Natarajan, V., Bishnoi, P.R., Kalogerakis, N., 1994. Induction phenomena in gas hydrate nucleation. Chem. Eng. Sci. 49 (13), 2075–2087. https://doi.org/10.1016/0009-2509(94)E0026-M.

Qi, W.H., Zhang, Z.S., Wu, T., 2020. Encapsulation of β-carotene in oleogel-in-water pickering emulsion with improved stability and bioaccessibility. Int. J. Biol. Macromol. 164, 1432–1442. https://doi.org/10.1016/j.ijbiomac.2020.07.227.

Qi, W.H., Li, T., Zhang, Z.S., et al., 2021. Preparation and characterization of oleogel-in-water pickering emulsions stabilized by cellulose nanocrystals. Food Hydrocoll. 110, 106206. https://doi.org/10.1016/j.foodhyd.2020.106206.

Raya, S.A., Saaid, I.M., Ahmed, A.A., et al., 2020. A critical review of development and demulsification mechanisms of crude oil emulsion in the petroleum industry. J. Pet. Explor. Prod. Technol. 10 (4), 1711–1728. https://doi.org/10.1007/s13202-020-00830-7.

Shi, B.H., Chai, S., Ding, L., et al., 2018. An investigation on gas hydrate formation and slurry viscosity in the presence of wax crystals. AIChE J. 64 (9), 3502–3518. https://doi.org/10.1002/aic.16192.

Song, G.C., Ning, Y.X., Li, Y.X., et al., 2020. Investigation on hydrate growth at the oil-water interface: In the presence of wax and kinetic hydrate inhibitor. Langmuir 36 (48), 14881–14891. https://doi.org/10.1021/acs.langmuir.0c02976.

Song, G.C., Ning, Y.X., Guo, P.H., et al., 2021. Investigation on hydrate growth at the oil-water interface: In the presence of wax and surfactant. Langmuir 37 (22), 6838–6845. https://doi.org/10.1021/acs.langmuir.1c01060.

Tong, S.K., Li, P.F., Lv, F.J., et al., 2023. Promotion and inhibition effects of wax on methane hydrate formation and dissociation in water-in-oil emulsions. Fuel 337, 127211. https://doi.org/10.1016/j.fuel.2022.127211.

Wang, D., Yang, D.L., Huang, C.L., et al., 2021. Stabilization mechanism and chemical demulsification of water-in-oil and oil-in-water emulsions in petroleum industry: A review. Fuel 286, 119390. https://doi.org/10.1016/j.fuel.2020.119390.

Wang, L., Chen, J.X., Ma, T.X., et al., 2024a. Experimental study of methane hydrate formation and agglomeration in waxy oil-in-water emulsions. Energy 288, 129945. https://doi.org/10.1016/j.energy.2023.129945.

Wang, L.M., Zheng, X., Xiao, P., et al., 2024b. Effects of wax on the formation of methane hydrate in oil-dominate systems: Experiments and molecular dynamics simulations. Fuel 357, 129748. https://doi.org/10.1016/j.fuel.2023.129748.

Wang, S.R., Yang, M.J., Liu, W.G., et al., 2016. Investigation on the induction time of methane hydrate formation in porous media under quiescent conditions. J. Petrol. Sci. Eng. 145, 565–572. https://doi.org/10.1016/j.petrol.2016.06.003.

Wang, W., Huang, Q.Y., Hu, S.J., et al., 2020a. Influence of wax on cyclopentane clathrate hydrate cohesive forces and interfacial properties. Energy & Fuels 34 (2), 1482–1491. https://doi.org/10.1021/acs.energyfuels.9b03543.

Wang, W., Huang, Q.Y., Zheng, H.M., et al., 2020b. Effect of wax on hydrate formation in water-in-oil emulsions. J. Dispersion Sci. Technol. 41 (12), 1821–1830. https://doi.org/10.1080/01932691.2019.1637751.

Wang, Y.J., Huang, Q.Y., Zhang, D.X., et al., 2022. Influence of asphaltenes on hydrate formation and decomposition in water-in-waxy oil emulsions. Energy & Fuels 36 (24), 14710–14722. https://doi.org/10.1021/acs.energyfuels.2c02959.

Xia, T.H., Xue, C.H., Wei, Z.H., 2021. Physicochemical characteristics, applications and research trends of edible pickering emulsions. Trends Food Sci. Technol. 107, 1–15. https://doi.org/10.1016/j.tifs.2020.11.019.

Xiao, Y.Y., Zhou, S.D., Li, X.Y., et al., 2023. Kinetic properties of CO_2 hydrate formation in the wax-containing system at different concentrations. Energy & Fuels 37 (4), 2972–2982. https://doi.org/10.1021/acs.energyfuels.2c03972.

Xu, H.F., Khan, F., Jung, S.H., et al., 2023. Probabilistic model for hydrate and wax risk assessment in oil and gas pipelines. Process Saf. Environ. Prot. 170, 11–18. https://doi.org/10.1016/j.psep.2022.11.083.

Yang, H., Jing, J.Q., Karimov, R., et al., 2024. Study on hydrate formation characteristics in crude oil-gas-water system considering emulsion gels. Fuel 364, 131052. https://doi.org/10.1016/j.fuel.2024.131052.

Zhang, D., Huang, Q., Li, R., et al., 2021. Effects of waxes on hydrate behaviors in water-in-oil emulsions containing asphaltenes. Chem. Eng. Sci. 244, 116831. https://doi.org/10.1016/j.ces.2021.116831.

Zhang, J., Li, C.X., Shi, L., et al., 2022. The formation and aggregation of hydrate in W/O emulsion containing different compositions: A review. Chem. Eng. J. 445, 136800. https://doi.org/10.1016/j.cej.2022.136800.

Zhang, J., Li, C.X., Yang, F., et al., 2023. Study on the influence mechanism of the interaction between waxes and asphaltenes on hydrate growth. Fuel 338, 127322. https://doi.org/10.1016/j.fuel.2022.127322.

Zheng, H.M., Huang, Q.Y., Wang, W., et al., 2017. Induction time of hydrate formation in water-in-oil emulsions. Ind. Eng. Chem. Res. 56 (29), 8330–8339. https://doi.org/10.1021/acs.iecr.7b01332.

Zhou, S.D., Chen, X.K., He, C.Y., et al., 2018. Experimental study on hydrate formation and flow characteristics with high water cuts. Energies 11 (10), 2610. https://doi.org/10.3390/en11102610.

Zhou, S.D., Guo, Y., Lian, M.M., et al., 2022. Study on the adhesion force between wax crystal particles and hydrate particles. ACS Omega 7 (6). https://doi.org/10.1021/acsomega.1c06458.

Zhou, S.D., Ren, Z.H., Guo, Y., et al., 2023. Effect of wax on cohesive behavior of gas hydrate under high pressure. Energy & Fuels 37 (7), 5303–5311. https://doi.org/10.1021/acs.energyfuels.2c04379.

Zi, M.C., Chen, D.Y., Wang, J., et al., 2019. Kinetic and rheological study of methane hydrate formation in water-in-oil emulsion: Effects of emulsion composition and silica sands. Fuel 255, 115708. https://doi.org/10.1016/j.fuel.2019.115708.